Advection by polytropic compressible turbulence

F. Ladeinde, E. E. O'Brien, X. Cai, and W. Liu
Department of Mechanical Engineering, SUNY at Stony Brook, Stony Brook, New York 11794-2300

(Received 7 February 1995; accepted 30 June 1995)

Direct numerical simulation (DNS) is used to examine scalar correlation in low Mach number, polytropic, homogeneous, two-dimensional turbulence ($M_s \leqslant 0.7$) for which the initial conditions, Reynolds, and Mach numbers have been chosen to produce three types of flow suggested by theory: (a) nearly incompressible flow dominated by vorticity, (b) nearly pure acoustic turbulence dominated by compression, and (c) nearly statistical equipartition of vorticity and compressions. Turbulent flows typical of each of these cases have been generated and a passive scalar field imbedded in them. The results show that a finite-difference based computer program is capable of producing results that are in reasonable agreement with pseudospectral calculations. Scalar correlations have been calculated from the DNS results and the relative magnitudes of terms in low-order scalar moment equations determined. It is shown that the scalar equation terms with explicit compressibility are negligible on a long time-averaged basis. A physical-space EDQNM model has been adapted to provide another estimate of scalar correlation evolution in these same two-dimensional, compressible cases. The use of the solenoidal component of turbulence energy, rather than total turbulence energy, in the EDQNM model gives results closer to those from DNS in all cases. © *1995 American Institute of Physics.*

I. INTRODUCTION

Recent studies of compressible turbulence in both decaying and forced[1,2] situations have enhanced our understanding of the roles of initial conditions, low Mach number asymptotics, energy flow, and spectral dynamics. However, fundamental studies of compressible turbulence that include dynamically passive scalars are scarce. In our work we use direct numerical simulation (DNS) to examine scalar transport by low Mach number, polytropic, two-dimensional turbulence ($M_s \leqslant 0.7$), for which the initial conditions, Reynolds, and Mach numbers have been chosen to produce (a) nearly incompressible flow dominated by vorticity, (b) nearly pure acoustic turbulence dominated by compression, and (c) nearly statistical equipartition of vorticity and compressions. The connection between initial velocity and pressure field data and the occurrence of any of the above regimes of flow have been elucidated by previous two-dimensional pseudospectral calculations of polytropic flow.[3] We have generated turbulent flows typical of each of these cases and imbedded a passive scalar field in them.

This paper is organized as follows. The asymptotic behavior of the flow variables is presented in Sec. II. This is followed in Sec. III by a discussion of consistent initial conditions for both velocity and scalar fields, followed by the presentation of two versions of the first and second moment equations for a homogeneously distributed scalar in compressible turbulence. Our numerical procedures are summarized in Sec. IV, while the extraction of turbulence and scalar statistics is discussed in Sec. V. In Sec. VI we validate our numerical procedure by comparing DNS calculations from our computer program with pseudospectral calculations by Ghosh and Matthaeus[3] (hereafter referred to as GM). We also examined the relative magnitudes of terms arising in the first- and second-order scalar moment equations and compared scalar correlations from DNS with those from an EDQNM (eddy-damped, quasinormal Markovian) model.

II. ASYMPTOTIC ORDERINGS

In this section, the asymptotic behavior of the flow variables is summarized. To this end, we consider the three perspectives presented by GM on the nature of low Mach number polytropic hydrodynamics. The following orderings have been reported: nearly incompressible,

$$|\mathbf{u}| = O(1), \quad |\nabla \times \mathbf{u}| = O(1), \quad |\nabla \cdot \mathbf{u}| = O(M_s^2),$$

$$\rho = O(1),$$

$$\delta\rho = O(M_s^2), \quad \delta p = p' + p^{\infty} = O(M_s^2), \quad M_s \ll 1;$$

modally equipartitioned compressive wave,

$$|\nabla \times \mathbf{u}| = O(1), \quad |\nabla \cdot \mathbf{u}| = O(1), \quad \mathbf{u}^I, \mathbf{u}^C = O(1),$$

$$\delta\rho = O(M_s);$$

compressive wave,

$$|\nabla \cdot \mathbf{u}| = O(1), \quad |\nabla \times \mathbf{u}| \to 0.$$

Concerning the asymptotic behavior of the scalar field ϕ, note that the temperature cannot be considered a passive scalar except in the asymptotic limit of nearly incompressible flow, as pointed out by Zank and Matthaeus.[4] The scaling results summarized above are unaffected by a dynamically passive scalar field. However, the scaling of ϕ will be determined by the velocity scaling and perhaps the initial scalar field. In the incompressible flow limit the initial scalar field has been shown to have only a minor effect.[5] Finally, we point out that in the DNS procedure the various equations (density, momentum, and scalar) are solved in the complete form, so that no terms are neglected on the basis of the asymptotic results. The initial density, velocity, and pressure

 1070-6631/95/7(11)/2848/10/$6.00

fields, and the Reynolds and Mach numbers ensure that the correct asymptotic results are obtained from the DNS calculations.

III. INITIAL CONDITIONS

The connection between initial velocity and pressure field data and the occurrence of any of the flow regimes listed in Sec. II have been elucidated by GM in two-dimensional pseudospectral calculations of polytropic flow. We generated turbulent flows typical of each of these cases and imbedded a passive scalar field in them. The initial conditions are classified as follows: SV/PS (Solenoidal Velocity/Pseudosound),

$$\nabla\cdot\mathbf{u}=0, \quad \rho(\mathbf{x})=1+\delta\rho_{\mathrm{PS}}(\mathbf{x}),$$

where $\delta\rho_{\mathrm{PS}}(\mathbf{x})$ is a "pseudosound" correction for initial density;
SV/CD (Solenoidal Velocity/Constant Density),

$$\nabla\cdot\mathbf{u}=0, \quad \rho(\mathbf{x})=1+\delta\rho_{\mathrm{PS}}(\mathbf{x})+\delta\rho_S(\mathbf{x});$$

RV/CD (Random Velocity/Constant Density),

$$\overline{|\nabla\cdot\mathbf{u}|}\approx\overline{|\nabla\times\mathbf{u}|}, \quad \rho(\mathbf{x})=1+\delta\rho_{\mathrm{PS}}(\mathbf{x})+\delta\rho_S(\mathbf{x});$$

LV/CD (Longitudinal Velocity/Constant Density),

$$\nabla\times\mathbf{u}=0, \quad \rho(\mathbf{x})=1+\delta\rho_{\mathrm{PS}}(\mathbf{x})+\delta\rho_S(\mathbf{x}).$$

Here $\delta\rho_S(\mathbf{x})$ is the acoustic density correction for initial density that satisfies

$$\delta\rho_S(\mathbf{x})=-\delta\rho_{\mathrm{PS}}(\mathbf{x})$$

in the initial state.

To generate the foregoing conditions numerically, we use finite difference and Fourier transform, as appropriate, moving back and forth from physical space to Fourier space. As an example, in order to generate a solenoidal velocity field, we carry out the following steps.

(1) Generate a random velocity field $\mathbf{u}$ in physical space, which satisfies the standard normal distribution.

(2) Transform $\mathbf{u}$ from physical space to $\hat{\mathbf{u}}$ in Fourier space.

(3) For SV/PS, SV/CD, and LV/CD conditions, decompose the velocity field $\hat{\mathbf{u}}$ in Fourier space into its incompressible part $\hat{\mathbf{u}}^{\mathbf{I}}$ and compressible part $\hat{\mathbf{u}}^{\mathbf{C}}$ according to the prescription

$$\hat{\mathbf{u}}^{\mathbf{C}}=\frac{\mathbf{k}\cdot\hat{\mathbf{u}}}{k^2}\cdot\mathbf{k},$$

$$\hat{\mathbf{u}}^{\mathbf{I}}=\hat{\mathbf{u}}-\hat{\mathbf{u}}^{\mathbf{C}}.$$

(4) Rescale $\hat{\mathbf{a}}$ as follows:

$$\hat{\mathbf{a}}(k_x,k_y)\leftarrow\hat{\mathbf{a}}(k_x,k_y)\sqrt{\frac{E(k_x,k_y)}{E^*(k_x,k_y)}},$$

where $\hat{\mathbf{a}}$ represents the randomly generated field, which is $\hat{\mathbf{u}}^{\mathbf{I}}$ (SV/PS and SV/CD), $\hat{\mathbf{u}}$ (RV/CD) or $\hat{\mathbf{u}}^{\mathbf{C}}$ (LV/CD). E_i is an imposed spectrum that was chosen to match that in GM and is specified as

$$E_i=E(i)=\begin{cases}1, & 1\leqslant k\leqslant\sqrt{12},\\ 0, & \text{otherwise},\end{cases}$$

where "i" is an index defined by $i-\frac{1}{2}\leqslant k<i+\frac{1}{2}$, with $k=\sqrt{k_x^2+k_y^2}$. The spectral energy of the randomly generated field is given by

$$E^*(k_x,k_y)=|\hat{\mathbf{a}}(k_x,k_y)|^2,$$

with a corresponding autocorrelation spectrum of

$$E_i^*=\sum_{i-1/2\leqslant k\leqslant i+1/2}|\hat{\mathbf{a}}(k_x,k_y)|^2.$$

(5) Transform scaled velocity $\hat{\mathbf{a}}$ to the physical space with an inverse FFT:

$\hat{\mathbf{u}}^{\mathbf{I}}\Rightarrow\mathbf{u}^{\mathbf{I}}$, SV/PS and SV/CD,

$\hat{\mathbf{u}}^{\mathbf{C}}\Rightarrow\mathbf{u}^{\mathbf{C}}$, LV/CD,

$\hat{\mathbf{u}}\Rightarrow\mathbf{u}$, RV/CD.

(6) Normalize $u_{\mathrm{rms}}=1$ by the transformation

$$\mathbf{u}(\mathbf{x})\leftarrow\frac{\mathbf{u}(\mathbf{x})}{u_{\mathrm{rms}}},$$

where

$$u_{\mathrm{rms}}=(\overline{|\mathbf{u}(\mathbf{x})|^2})^{1/2}.$$

For constant density condition (CD) cases, we set the initial density to

$$\rho(\mathbf{x},0)=1.0,$$

and obtain pressure from

$$p=\rho^{\gamma}.$$

For the pseudosound condition (PS), we obtain $\delta\rho_{\mathrm{PS}}(\mathbf{x})$ by first solving for the pressure fluctuation p from the Poisson equation for the incompressible component of the initial velocity field:

$$\nabla^2 p=-\gamma M_1^2\nabla\cdot(\mathbf{u}^{\mathbf{I}}\cdot\nabla\mathbf{u}^{\mathbf{I}}),$$

where the right-hand side in this equation is due entirely to the solenoidal velocity component $\mathbf{u}^{\mathbf{I}}$ from a random number. It is pointed out that unphysical pressures were obtained from this equation when Mach number exceeds 0.6, a result that was confirmed by GM (oral communication with Dr. Ghosh). The nearly incompressible asymptotic theory breaks down at Mach numbers greater than 0.6

The pseudosound density fluctuation is obtained from the relation

$$\delta\rho_{\mathrm{PS}}=\frac{1}{\gamma}p.$$

We obtain the initial pressure and density by

$$P=1+p, \quad \rho=1+\delta\rho_{\mathrm{PS}}.$$

Initial conditions for scalar $\phi(\mathbf{x},0)$ were generated as a random variable $\psi(\mathbf{k},0)$, in Fourier space, of the form

$$\psi(\mathbf{k},0)=\Phi(k)\exp[2\pi i\theta(\mathbf{k})],$$

where $\theta(\mathbf{k})$ is a uniformly distributed random number between 0 and 1. The PDF of θ is a box of height 1 that varies from 0 to 1 along k. Here $\Phi(\mathbf{k},0)$ is prescribed as

$$\Phi(\mathbf{k},0)=\exp[-c(k_x^2+k_y^2)],$$

where $|k_x|,|k_y|\leqslant 4$, and $c=0.1$. Larger values of c give narrower Gaussian profiles, which are undesirable numerically, as they require more grid points for resolution. For the incompressible case,[5] the eventual scalar evolution is fairly insensitive to the initial scalar field, and any well-behaved $\phi(\mathbf{x},0)$ is suitable. It will be assumed that this is the case in the present studies, with partial justification coming from the fairly low Mach numbers. To ensure that $\psi(\mathbf{k},0)$ is real when transformed to the physical space, we set

$$\psi(-\mathbf{k},0)=\psi^*(\mathbf{k},0),$$

where $\psi^*(\mathbf{k},0)$ is the complex conjugate of $\psi(\mathbf{k},0)$. Finally, we transform $\psi(\mathbf{k},0)$ into the physical space and normalize all nodal values of ϕ by dividing by the rms value $(\Sigma\psi^2/N)^{1/2}$, where N is the number of nodes in the grid.

For homogeneous, isotropic turbulence and scalar field $\phi(\mathbf{x},t)$ obeying the conservation equations given in (5) below, the first- and second-order moments of ϕ satisfy the following equations (1) and (3). The density-weighted scalar, $\rho\phi$, satisfies first and second moment equations (2) and (4):

$$\frac{\partial\bar{\phi}}{\partial t}=\overline{(\nabla\cdot\mathbf{u})\phi'}+D_\phi\,\overline{\frac{\partial\ln\rho}{\partial x_i}\frac{\partial\phi'}{\partial x_i}}, \tag{1}$$

$$\frac{\partial\overline{\rho\phi}}{\partial t}=0, \tag{2}$$

$$\frac{\partial\overline{(\phi')^2}}{\partial t}=\overline{(\nabla\cdot\mathbf{u})(\phi')^2}-2D_\phi\,\overline{\frac{\partial\phi'}{\partial x_j}\frac{\partial\phi'}{\partial x_j}}+D_\phi\,\overline{\frac{\partial(\phi')^2}{\partial x_j}\frac{\partial\ln\rho}{\partial x_j}}, \tag{3}$$

$$\begin{aligned}\frac{\partial\overline{(\rho'\phi')^2}}{\partial t}=&-\overline{(\nabla\cdot\mathbf{u})(\rho'\phi')^2}-2D_\phi\,\overline{\frac{\partial\rho'\phi'}{\partial x_j}\frac{\partial\rho'\phi'}{\partial x_j}}\\&-2\overline{\rho\phi}\;\overline{(\nabla\cdot\mathbf{u})\rho'\phi'}+2D_\phi\overline{\rho\phi}\\&\times\overline{\frac{\partial\rho'\phi'}{\partial x_j}\frac{\partial\ln\rho}{\partial x_j}}+D_\phi\,\overline{\frac{\partial(\rho'\phi')^2}{\partial x_j}\frac{\partial\ln\rho}{\partial x_j}}.\end{aligned} \tag{4}$$

In these equations an overbar means an ensemble or spatial average, a prime indicates a fluctuating variable with zero mean, and the diffusivity D_ϕ has been taken as constant. It should be noted that the use of a density-weighted concentration average $\overline{\rho\phi}$, rather than $\bar{\phi}$ itself, simplifies the behavior of the scalar mean quantity [Eqs. (1) and (2)], but at the expense of a more complex expression for scalar variance [Eqs. (3) and (4)], arising from the molecular diffusion process, which is assumed to be Fickian. In Sec. VI, the discussion of results, our finite-difference based computer program is used to evaluate each of the terms on the right-hand side of Eqs. (1), (3), and (4). One purpose is to compare the relative importance of velocity divergence-scalar correlations and density gradient-scalar gradient correlations, both of which are unique to compressible flow. Another is to evaluate the "compressible" molecular diffusion terms in (3) and (4) *vis a vis* the traditional dissipation terms, which have been placed as the second terms on the right-hand side of (3) and (4), respectively. Note also the difference in sign of the first terms on the right-hand side of Eqs. (3) and (4), which concern the correlation between velocity divergence and squared scalar fluctuations. These terms play analogous roles in (3) and (4), respectively, the difference in sign is a consequence of density weighting since density fluctuations and velocity divergence fluctuations roughly counterbalance each other. Our numerical results, discussed in Sec. VI, confirm this behavior.

IV. NUMERICAL PROCEDURE

Our computer program has been developed to include the complete (three-dimensional) Navier–Stokes and energy equations and a scalar transport equation. However, in the present study, the program was modified to be compatible with the polytropic conditions in GM. Unlike in GM, where the equations are solved with the pseudospectral method, we use a finite-difference-based essentially nonoscillatory (ENO) procedure,[6] to assess the performance of the latter for low Mach number turbulence. Compared to the pseudospectral method, the ENO scheme has better nonlinear stability properties, which make it more suitable for fundamental work on supersonic and hypersonic flows. The specific numerical approach that we have used follows Shu and Osher,[7,8] Shu,[9] and Shu *et al.*,[10] although the following modifications to Shu's procedure were necessary in order to be compatible with the scalings in GM and to include scalar advection.

(1) The initial velocities in GM, which were generated as described earlier, were multiplied by the scale factor $\sqrt{\gamma}M_1$ to obtain a consistent scaling of the flow equations.

(2) We removed the energy equation in Shu's procedure and directly apply the polytropic relation:

$$p=\rho^\gamma.$$

(3) We used a stencil that is biased for central differencing, instead of an adaptive stencil.

(4) We added a scalar equation to the equation set considered by Shu or GM. The resulting equations for DNS can be written as

$$\mathbf{q}_t+\mathbf{f}(\mathbf{q})_x+\mathbf{g}(\mathbf{q})_y=\mathbf{r}(\mathbf{q})_x+\mathbf{s}(\mathbf{q})_y, \tag{5}$$

where

$$\mathbf{q}=\begin{pmatrix}\rho\\ \rho u\\ \rho v\\ \rho\phi\end{pmatrix},\quad \mathbf{f}(\mathbf{q})=u\mathbf{q}+\begin{pmatrix}0\\ p\\ 0\\ 0\end{pmatrix},$$

$$\mathbf{g}(\mathbf{q})=v\mathbf{q}+\begin{pmatrix}0\\ 0\\ p\\ 0\end{pmatrix},$$

and

$p=\rho^{\gamma}$.

Compared to the expressions given in Shu,[10] the vectors $\mathbf{r}(\mathbf{q})$ and $\mathbf{s}(\mathbf{q})$ are only slightly modified by the inclusion of the scalar diffusion term $D_{\phi}\phi_{,jj}$, where D_{ϕ} is scalar diffusivity. The Jacobians of the matrices $\partial\mathbf{f}/\partial\mathbf{q}$ and $\partial\mathbf{g}/\partial\mathbf{q}$ were evaluated and used in the ENO procedure, as were their right and left eigenvectors. For a better accuracy of the ENO solution, under the relatively low Mach number conditions in our study, we implemented the modification in Shu[9] pertaining to a central stencil. Domain is a square of length 2π and a grid resolution of 64×64 is used, in order to match the conditions in GM. Calculations with 128×128 were also carried out for the scalar studies and to show grid independence of the GM results.

V. COMPUTATION OF TURBULENCE AND SCALAR STATISTICS

The primary dependent variables from DNS are ρ, ρu, ρv, and $\rho\phi$. From these, the turbulence and scalar statistics are computed. The definitions of the various turbulence quantities, as given below, follow those in GM. The exceptions are the quantities with the subscript "turb," which are quantities from which the effect of back transfer has been removed. In our work, removal was accomplished by excluding the fundamental mode from the solenoidal fields, as defined below. The procedure in GM is more involved, as it includes some manipulations of the compressible modes as well. The definitions of the various turbulence and scalar quantities are given below, where an overbar indicates spatial averaging and angular brackets indicate time averaging: Average internal energy,

$$E_{\text{int}}=\frac{\overline{\rho^{\gamma}}-\bar{\rho}^{\gamma}}{M_1^2\gamma(\gamma-1)};$$

average kinetic energy,

$$E_{\text{kin}}=\frac{\overline{\rho\mathbf{u}\cdot\mathbf{u}}}{2};$$

local sound speed (dimensionless),

$$c_s(\mathbf{x})=M_1^{-1}\rho(\mathbf{x})^{(\gamma-1)/2};$$

sonic Mach number of the turbulent flow,

$$M_s=u_{\text{rms}}/[\overline{c_s(\mathbf{x})}];$$

density fluctuation,

$$\Delta\rho=(\overline{\rho^2-\bar{\rho}^2})^{1/2};$$

Reynolds number,

$$\text{Re}=\frac{u_{\text{rms}}}{\nu};$$

eddy turnover time,

$$T_E=t\langle u_{\text{rms}}\rangle\sqrt{\gamma}M_1,$$

where

$$\langle u_{\text{rms}}\rangle=\frac{1}{t}\int_0^t u_{\text{rms}}\cdot dt;$$

longitudinal velocity component,

$$U^L=\{\overline{|\text{FFT}^{-1}(\hat{\mathbf{u}}^{\mathbf{C}})|^2}\}^{1/2};$$

transverse velocity component,

$$U^T=\{\overline{|\text{FFT}^{-1}(\hat{\mathbf{u}}^{\mathbf{I}})|^2}\}^{1/2};$$

turbulent solenoidal velocity,

$$U^T_{\text{turb}}=(\overline{|\text{FFT}^{-1}[\hat{\mathbf{u}}^{\mathbf{I}}_{\mathbf{k}\neq\mathbf{1}}(\mathbf{x})]|^2})^{1/2};$$

turbulent total velocity,

$$U_{\text{turb}}=(\overline{\{\text{FFT}^{-1}[\hat{\mathbf{u}}(\mathbf{x})-\hat{\mathbf{u}}^{\mathbf{I}}_{\mathbf{k}=\mathbf{1}}(\mathbf{x})]\}^2})^{1/2};$$

turbulent Mach number,

$$M_{\text{turb}}=\frac{U_{\text{turb}}}{\overline{c_s(\mathbf{x})}};$$

internal energy spectrum,

$$P_{\text{int}}(i)=\frac{1}{m}\sum_{i-1/2\leqslant k<i+1/2}\left|\text{FFT}\left(\sqrt{\frac{\rho^{\gamma}}{M_1^2\gamma(\gamma-1)}}\right)\right|^2;$$

kinetic energy spectrum,

$$P_{\text{kin}}(i)=\frac{1}{m}\sum_{i-1/2\leqslant k<i+1/2}\frac{1}{2}|\text{FFT}(\sqrt{\rho}\mathbf{u})|^2,$$

where m refers to the number of modes in an annulus for the bin in spectral space.

We define scalar correlation by

$$R(\mathbf{r})=\overline{\phi(\mathbf{x})\phi(\mathbf{x}+\mathbf{r})}$$

and obtain one-dimensional (x_1,x_2) correlations from DNS solutions via the expressions

$$R_1(x_1)=\frac{1}{N}\sum_{j=1}^{N_y}\sum_{i=1}^{Nx}\phi(x_i,x_j)\phi(x_i+x_1,x_j)$$

and

$$R_2(x_2)=\frac{1}{N}\sum_{j=1}^{N_y}\sum_{i=1}^{Nx}\phi(x_i,x_j)\phi(x_i,x_j+x_2).$$

In terms of $r=\sqrt{x^2+y^2}$, scalar correlation is expressed as

$$R(r)=\frac{1}{N}\sum_{j=1}^{N_y}\sum_{i=1}^{Nx}\phi(x_i,x_j)\times\sum_{m=1}^{N_1}\sum_{n=1}^{N_2}\phi(x_i+\Delta x_m,x_j+\Delta y_n),$$

where m, n, N_1, and N_2 are such that

$$(\Delta x_m,\Delta y_n)\in\{[0,\Delta x(N_x-1)]\times[0,\Delta y(N_y-1)]\}$$

and

$$r=\sqrt{\Delta x_m^2+\Delta y_n^2}.$$

The results presented are for $R(r)$.

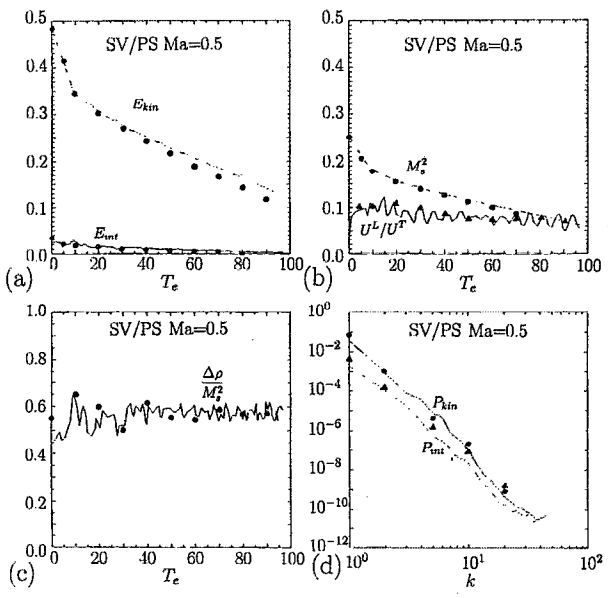

FIG. 1. Characteristics of the M_s=0.5 SV/PS simulation. Results from the present work (lines) are compared with the pseudospectral calculations in GM (dots). In (a) the variation with time of the kinetic ($E_{\rm kin}$) and internal ($E_{\rm int}$) energy are shown, where the dots denote results of GM and the lines denote results from present studies. In (b) the circular and triangular dots denote the results of GM for M_s^2 and U^L/U^T, respectively. (c) shows the variation with time of $\Delta\rho/M_s^2$, the dots denote results of GM and the lines denote results from present studies. In (d) the circular and triangular dots denote the results of GM for $P_{\rm kin}$ and $P_{\rm int}$, respectively. The results in (d) are for $T_e \simeq 20.5$. The symbols are defined in Sec. V.

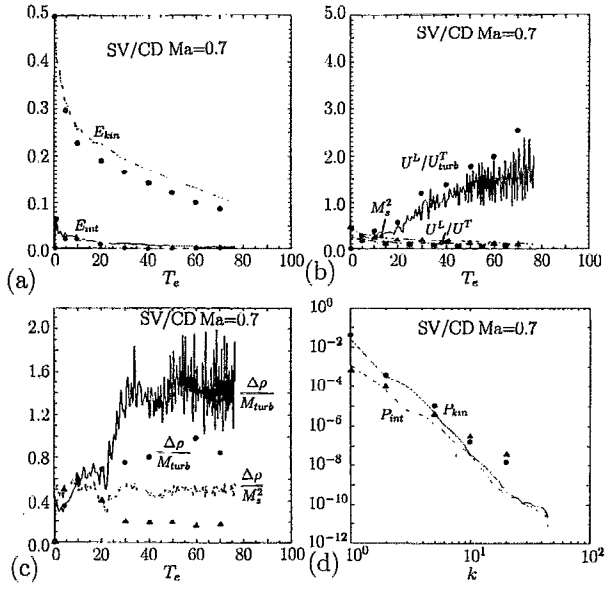

FIG. 2. Characteristics of the M_s=0.7 SV/CD simulation. Results from the present work (lines) are compared with the pseudospectral calculations in GM (dots). In (a) the variation with time of the kinetic ($E_{\rm kin}$) and internal ($E_{\rm int}$) energy are shown, where the dots denote results of GM and the lines denote results from present studies. In (b) the circular, triangular, and square dots denote the results of GM for $U^L/U^T_{\rm turb}$, M_s^2, and U^L/U^T, respectively. In (c) the circular and triangular dots denote the results of GM for $\Delta\rho/M_{\rm turb}$ and $\Delta\rho/M_s^2$, respectively. In (d) the circular and triangular dots denote the results of GM for $P_{\rm kin}$ and $P_{\rm int}$, respectively. The results in (d) are for $T_e \simeq 20.5$. The symbols are defined in Sec. V.

VI. RESULTS

In order to validate our finite difference-based computer program, calculations from it are compared with the pseudospectral calculations of GM in Figs. 1–4, which correspond to the cases SV/PS, SV/CD, RV/CD, and LV/CD, respectively. Comparisons are made for the quantities $E_{\rm kin}$, $E_{\rm int}$, M_s^2, $\Delta\rho/M_s^2$, $P_{\rm kin}$, $P_{\rm int}$, $\Delta\rho/M_{\rm turb}$, U^L/U^T, and $U^L/U^T_{\rm turb}$. A discussion of the physics of the flows in Figs. 1–4 is available in GM and is not repeated here.

An examination of these figures shows that our program is capable of producing excellent results. For instance, the calculations for the quantities, M_s^2, $\Delta\rho/M_s^2$, $\Delta\rho/M_{\rm turb}$, U^L/U^T, and $U^L/U^T_{\rm turb}$ agree well with theoretical scaling results. Further, quantitative agreement with GM is also apparent for many of the quantities. Differences in the treatment of back transfer in the two studies might explain the quantitative discrepancies that are observed in a few of the calculations. Note that accurate results for the GM problem are those that reproduce the scalings in Sec. II of this paper. Thus, the actual numbers in our calculations do not have to match those in GM exactly, for us to have accurate calculations. Nevertheless, the details of the results are of interest.

Scalar transport by homogeneous turbulence has been studied for almost as long as homogeneous turbulence itself;[11] it has been widely used to evaluate closure models and to test theoretical concepts that are often more tractable for a scalar than for vector velocity or vorticity.[12] Most of the published results have been concerned with incompressible, three-dimensional turbulence. In this paper we explore numerically the role of compressibility on some aspects of scalar transport when the fields are two dimensional. In the combustion literature, because the advective terms are simplified, it is common practice to use a density-weighted averaging process for concentration fields, even though molecular diffusion terms become much more complicated in this formulation. Our results evaluate all terms in the mean and intensity scalar equations for both non-density-weighted [Eqs. (1) and (3)] and density-weighted [Eqs. (2) and (4)] concentrations.

Figures 5–17 display the effects of compressibility on the following aspects of scalar transport. They show scalar flux, scalar correlation, and the calculations of the various terms in Eqs. (1)–(4) for the cases SV/PS, M_s=0.5 (Nearly Incompressible), RV/CD, M_s=0.7 (Modally Equipartitioned Compressible), and LV/CD, M_s=0.5 (Compressive Wave). These cases were chosen in order to represent various regimes of compressibility.

Concerning the temporal behavior of the terms in (1)–(4), we have observed a high-frequency oscillatory behavior for the density, velocity, and scalar fields. An exception (not shown) is the dissipation term $\epsilon_\phi = 2D_\phi(\partial\phi'/\partial x_j)(\partial\phi'/\partial x_j)$ in (3), which tends to have a relatively smooth variation with time. This oscillatory phenomenon was observed using both coarse and fine grids, suggesting that the oscillations are physical and not artifacts of the numerical procedure. Similar nonmonotonic behavior can be observed in the velocity and density calculations of GM.

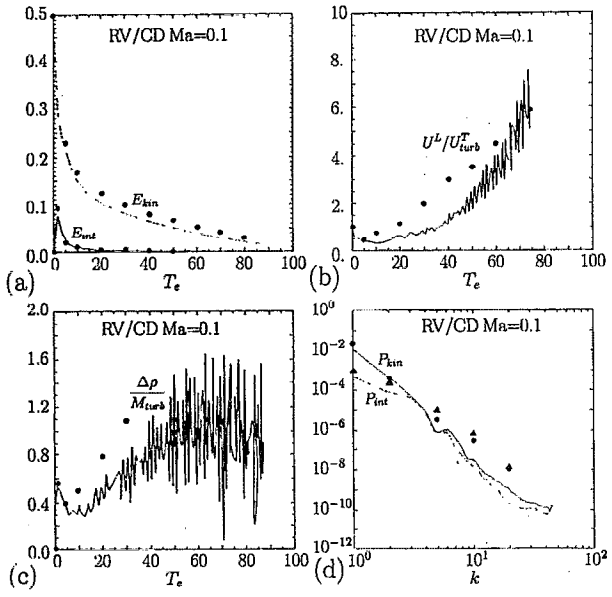

FIG. 3. Characteristics of the M_s=0.1 RV/CD simulation. Results from the present work (lines) are compared with the pseudospectral calculations in GM (dots). In (a) the variation with time of the kinetic (E_{kin}) and internal (E_{int}) energy are shown, where the dots denote results of GM and the lines denote results from present studies. In (b) the variation with time of U^L/U^T_{turb} is shown, where the dots denote results of GM and the lines denote results from present studies. (c) shows the variation with time of $\Delta\rho/M_{turb}$; the dots denote results of GM and the lines denote results from present studies. In (d) the circular and triangular dots denote the results of GM for P_{kin} and P_{int}, respectively. The results in (d) are for $T_e \simeq 20.5$. The symbols are defined in Sec. V.

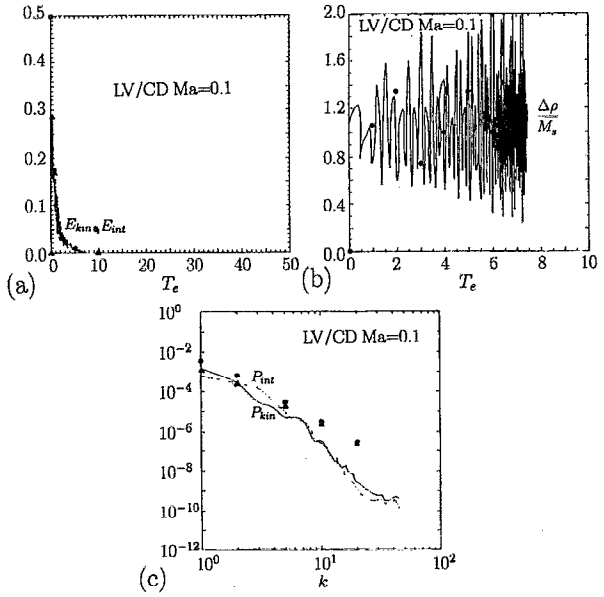

FIG. 4. Characteristics of the M_s=0.1 LV/CD simulation. Results from the present work (lines) are compared with the pseudospectral calculations in GM (dots). In (a) the variation with time of the kinetic (E_{kin}) and internal (E_{int}) energy are shown, where the dots denote results of GM and the lines denote results from present studies. (b) shows the variation with time of $\Delta\rho/M_s$, the dots denote results of GM and the lines denote results from present studies. In (c) the circular and triangular dots denote the results of GM for P_{kin} and P_{int}, respectively. The results in (c) are for $T_e \simeq 4.0$. The symbols are defined in Sec. V.

In order to evaluate the magnitude of the other terms in (3), $\partial\overline{(\phi')^2}/\partial t$, $\overline{(\nabla\cdot\mathbf{u})(\phi')^2}$, and $D_\phi\overline{[\partial(\phi')^2/\partial x_j](\partial \ln\rho/\partial x_j)}$, which all show high-frequency oscillations (Fig. 5), we have presented the same data again in Fig. 6, with the high-frequency oscillations filtered out. We filter by averaging over a time interval and plotting the sliding averages.

The results shown in Figs. 5 and 6 for the scalar variance equation (3), are for the case RV/CD, M_s=0.7. Note that the terms in this equation have been scaled with the scalar dissipation ϵ_ϕ. It is evident from Fig. 6 that, for the filtered quantities, and ignoring the initial transients, the rate of decay of the mean squared scalar is equal, effectively, to ϵ_ϕ, as it is for incompressible turbulence. This means that scalar variance evolution is not much affected directly by compressibility, except locally in time through the temporal oscillations. Of course, the scalar gradients of which ϵ_ϕ is comprised may be sensitive to compressibility effects. The behavior of the scalar quantities in the other two types of turbulence (SV/PS and LV/CD) are similar.

The numerical calculation of Eq. (1) is shown in Fig. 7 for the modally equipartitioned compressible case (RV/CD, M_s=0.7). It is evident that the diffusion term $D_\phi\overline{(\partial \ln\rho/\partial x_j)(\partial\phi'/\partial x_j)}$ is negligibly small and that $\partial\rho/\partial t$ is balanced by $\overline{(\nabla\cdot\mathbf{u})\phi'}$ alone. This result is valid for all the turbulence cases studied. It is clear from (1) that homogeneity does not guarantee a constant mean concentration $\bar{\phi}$ in compressible flows, but from Fig. 8, the filtered version of Eq. (1), it is evident that the filtered, asymptotic value of $\bar{\phi}$ is indeed constant in the compressible flow cases we have studied.

The computed values of $\overline{\rho\phi}$ (not shown) are smaller than 10^{-6} for all cases investigated. This is in agreement with the requirements of homogeneity and Eq. (2), since the initial fields in our studies have a zero value for $\rho\phi$.

Terms in the density-averaged variance equation (4)

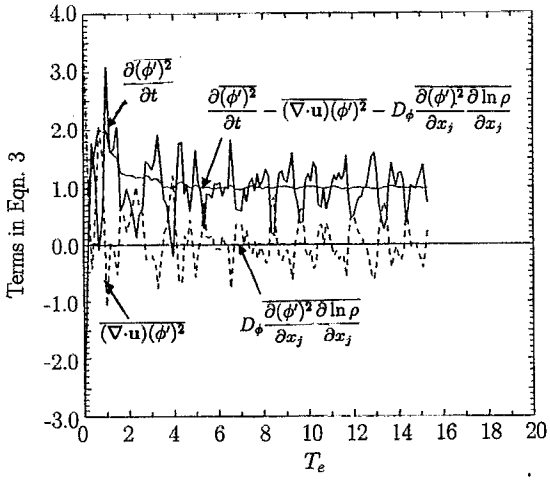

FIG. 5. Temporal variation of the terms in Eq. (3) normalized by ϵ_ϕ for RV/CD M_s=0.7 using a 128×128 grid. The results in this figure have been normalized by the dissipation term $\epsilon = 2D_\phi\overline{(\partial\phi'/\partial x_j)(\partial\phi'/\partial x_j)}$. The unfiltered case.

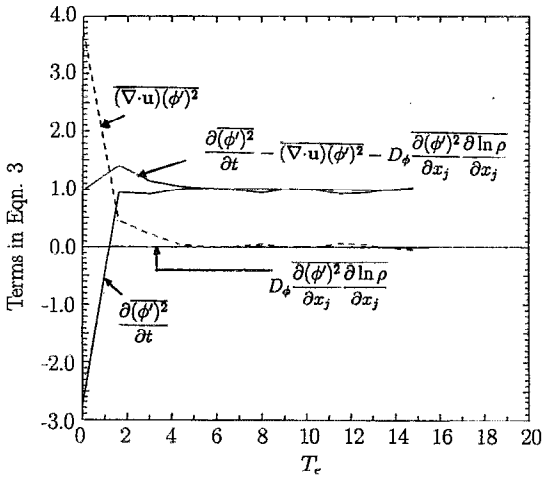

FIG. 6. Temporal variation of the terms in Eq. (3) for RV/CD M_s=0.7 using a 128×128 grid. The results in this figure have been normalized by the dissipation term $\epsilon = 2D_\phi(\partial\phi'/\partial x_j)(\partial\phi'/\partial x_j)$. The filtered case.

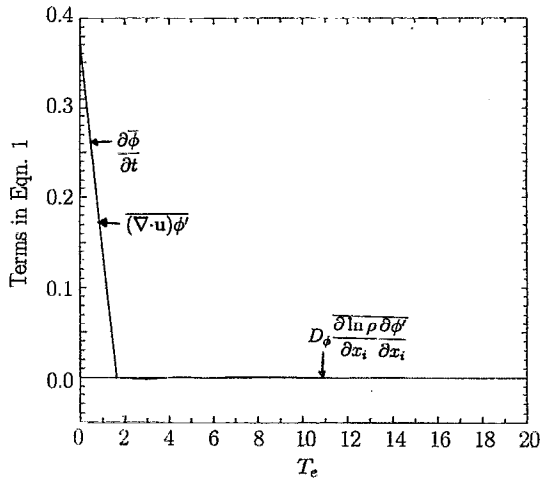

FIG. 8. Temporal variation of the terms in Eq. (1) for RV/CD M_s=0.7 using a 128×128 grid. Absolute values of the various quantities are shown. The filtered case.

have also been calculated. Because $\overline{\rho\phi}$ is zero, the third and fourth terms on the right-hand side of (4) should be zero, which we have observed to be the case from our numerical calculations. Moreover, the divergence term and the remaining density term (first and fifth, respectively) have an insignificant contribution for eddy turnover times greater than 3, compared to the dissipation term (second). This result is true for all the cases we computed (SV/PS, M_s=0.5, RV/CD, M_s=0.7, and LV/CD, M_s=0.5) and it implies that, as a practical matter, density averaging in a homogeneous system does not complicate scalar variance evolution. As anticipated in Sec. III, we note, without showing the result, that the filtered term $\overline{(\nabla\cdot\mathbf{u})(\rho'\phi')^2/\epsilon_\psi}$ in (4), where $\epsilon_\psi = 2D_\phi[\partial(\rho'\phi')/\partial x_j][\partial(\rho'\phi')/\partial x_j]$, is virtually the mirror image about the time axis of the term $\overline{(\nabla\cdot\mathbf{u})(\phi')^2/\epsilon_\phi}$, which is displayed in Fig. 6.

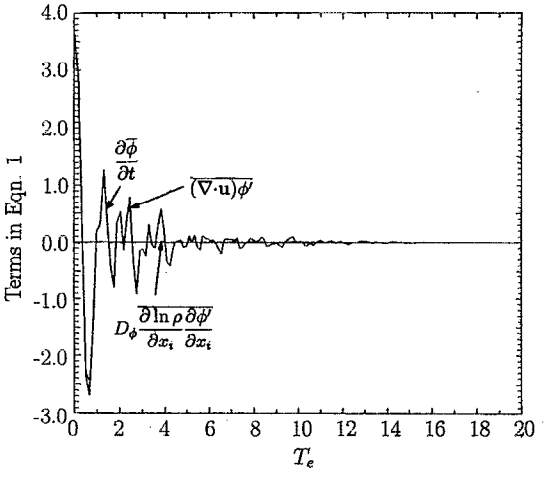

FIG. 7. Temporal variation of the terms in Eq. (1) for RV/CD M_s=0.7 using a 128×128 grid. Absolute values of the various quantities are shown. The unfiltered case.

Scalar flux results are shown in Figs. 9–11 for RV/CD, M_s=0.7. Figure 9 pertains to one-point data for the scalar flux $\overline{\mathbf{u}\phi'}$, whereas the corresponding two-point velocity-scalar covariance results are given in Figs. 10 and 11. In order to isolate compressibility effects in Fig. 9, the solenoidal $\overline{(u_j')^s\phi}$, dilatational $\overline{(u_j')^d\phi}$, and total $\overline{(u_j')^T\phi}$ components of scalar flux are plotted individually. They are scaled by the quantity $u_{\rm rms}^T\phi_{\rm rms}$.

Although strict isotropy requires that all three fluxes be identically zero, numerical computations of compressible turbulence have found it difficult to attain isotropy.[13] In our calculations of two types of turbulence the dilatational contribution is smaller than the solenoidal and both contributions are oscillatory (Fig. 9). In a compressible, turbulent, homogeneous shear flow with uniform mean scalar gradient,[14] it has been shown that the dilatational contribution to scalar flux is negligible. Our result is consistent with this finding.

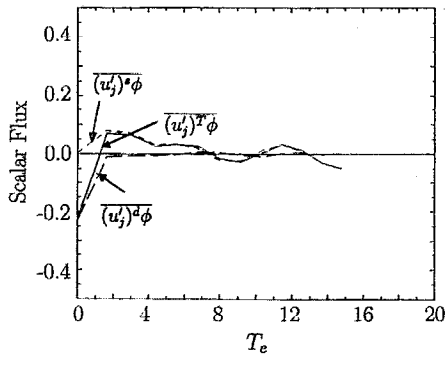

FIG. 9. Scalar flux for RV/CD M_s=0.7 using a 128×128 grid. Scalar flux in the x direction is shown. Similar behavior is observed for the y direction. Note that the results in this figure have been normalized by the quantity $u_{\rm rms}^T\phi_{\rm rms}$.

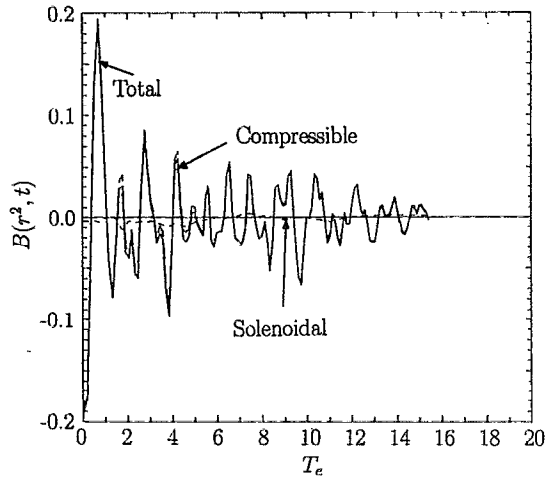

FIG. 10. Velocity-scalar covariance for RV/CD M_s=0.7 using a 128×128 grid. Results are presented in terms of $B(r^2,t)$ at r=0.5 and are normalized by $u^T_{\rm rms}\phi_{\rm rms}$. The values of $B(r^2,t)$ evaluated with the compressible, solenoidal, and total velocities are shown. Note that the time t in $B(r^2,t)$ is the eddy turnover time T_e.

The velocity-scalar two-point correlation function for isotropic fields can be written[15] as

$$\overline{u_j'\phi(\mathbf{r},t)}=B(r^2,t)r_j.$$

The behavior of $B(r^2,t)$ for the case RV/CD, M_s=0.7 is shown in Fig. 10 for r=0.5 and, in Fig. 11, for its dependence on r and t. The various flux terms oscillate about zero for all cases considered. While a zero mean is expected for the incompressible (solenoidal) component, the results in this paper show that compressibility does not change this behavior, as far as the time-averaged values are concerned. However, the amplitude and periodicity of the oscillation about zero depend strongly on compressibility.

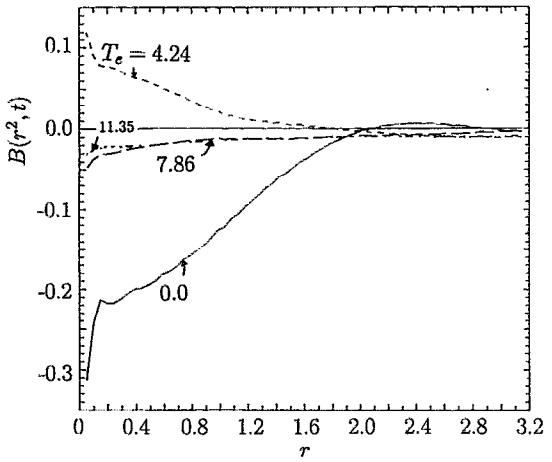

FIG. 11. Velocity-scalar covariance for RV/CD M_s=0.7 using a 128×128 grid. Results are presented in terms of $B(r^2,t)$ for $0\leqslant r\leqslant 3.2$ and are normalized by $u^T_{\rm rms}\phi_{\rm rms}$. The values of B at eddy turnover times of t=0.0, 4.24, 7.86, and 11.35 are shown. Note that the time t in $B(r^2,t)$ is the eddy turnover time T_e. The total velocity (compressible plus solenoidal) are used to compute B.

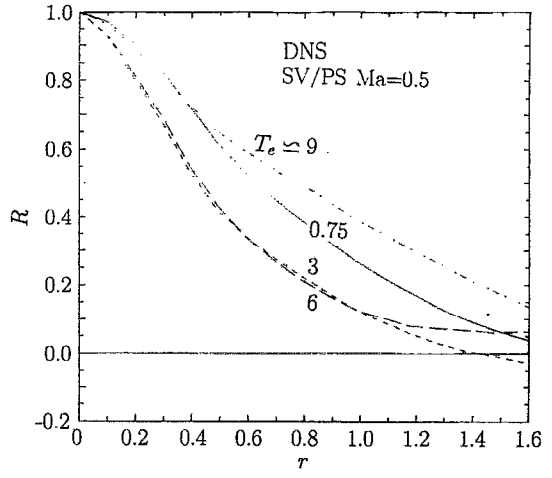

FIG. 12. Variation of scalar correlation R with separation distance r for the M_s=0.5 SV/PS simulation. DNS results are shown in this figure for eddy turnover times T_e of 0.75, 3, 6, and 9.

Scalar correlation results obtained from DNS are presented in Figs. 12–17. As far as we know there are no data with which to compare these results. Figures 12, 14, and 16 show, respectively, the evolved shape of the scalar correlation function at times T_e approximately equal to 0.75, 3.0, 6.0, and 9.0 for the cases SV/PS (M_s=0.5), SV/CD (M_s=0.7), and RV/CD (M_s=0.7).

We have adopted a physical-space EDQNM model,[16] which has had some success in describing the evolution of low-order scalar moments in three-dimensional, incompressible, homogeneous turbulence,[5] to provide another estimate of scalar correlation evolution in these same two-dimensional, compressible cases. The adaptation consists entirely in changing the kernel of the eddy diffusivity, $\nu_\in$, to its two-dimensional form,

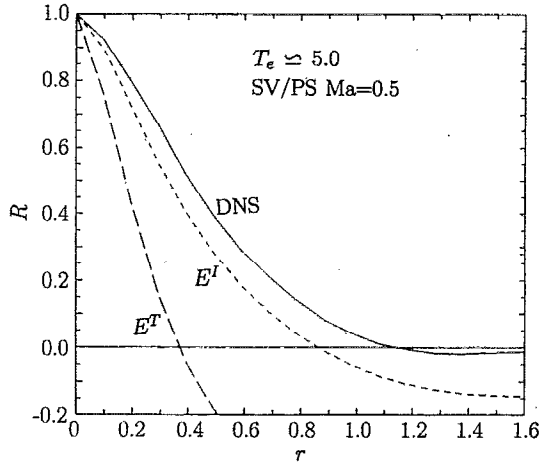

FIG. 13. Variation of scalar correlation R with separation distance r for the M_s=0.5 SV/PS simulation. DNS results are compared with results from an EDQNM model using total turbulence energy (E^T) and solenoidal part of turbulence energy (E^I). Results in this figure were obtained at T_e≃5.0.

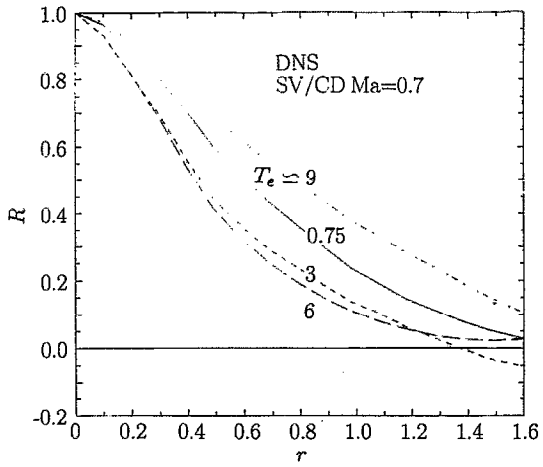

FIG. 14. Variation of scalar correlation R with separation distance r for the M_s=0.7 SV/CD simulation. DNS results are shown in this figure for eddy turnover times T_e of 0.75, 3, 6, and 9.

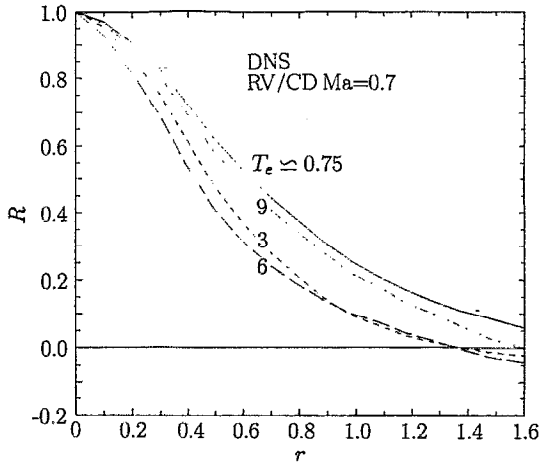

FIG. 16. Variation of scalar correlation R with separation distance r for the M_s=0.7 RV/CD simulation. DNS results are shown in this figure for eddy turnover times T_e of 0.75, 3, 6, and 9.

$$v_\epsilon = \sqrt{\pi}\int_0^\infty \theta(k,t)E(k,t)\left[1-\left(\frac{2}{kr}\right)J_1(kr)\right]dk.$$

Here $J_1(kr)$ is the Bessel function of order 1. The definition of the other terms in this equation can be found in Jiang and O'Brien.[17] A finite element code is used to solve the equation for the same three cases as were subjected to DNS; comparisons are presented for each case in Figs. 13, 15, and 17. The two EDQNM model solutions for each case are a consequence of interpreting[18] the energy spectrum as either the total energy spectrum $E^T(k,t)$ or the incompressible energy spectrum, $E^I(k,t)$.

The original model was developed for incompressible turbulence in which $E^T(k,t)$ and $E^I(k,t)$ are identical. There is no evidence to support the notion that scalar transport by compressible modes follows the EDQNM model, but there is speculation that these modes are relatively ineffective at scalar transport,[14] an idea consistent with the observation[19] that compressible modes tend to dominate at the high wave number end of the spectrum. On the other hand, if the compressible modes are effective scalar transporters, it is likely that the EDQNM model will be an unsatisfactory representation of the phenomenon, since the mechanisms of transport must be quite different from those of the solenoidal components and an EDQNM closure is potentially nonrealizable in the presence of wave phenomenon.[20] The two EDQNM solutions for each case in Figs. 13, 15, and 17 represent an exploration of this issue. In each case, except for the large r region of the correlation in Fig. 17, the use of $E^I(k,t)$ gives results closer to those from DNS.

The reader should note the nonmonotonic temporal behavior in $R(r,t)$ in Figs. 12–17. For example, for SV/PS (Fig. 12), $R(0.8,t)$ has the approximate values 0.37, 0.22, 0.2, and 0.48 for t=0.75, 3, 6, and 9. This may be a conse-

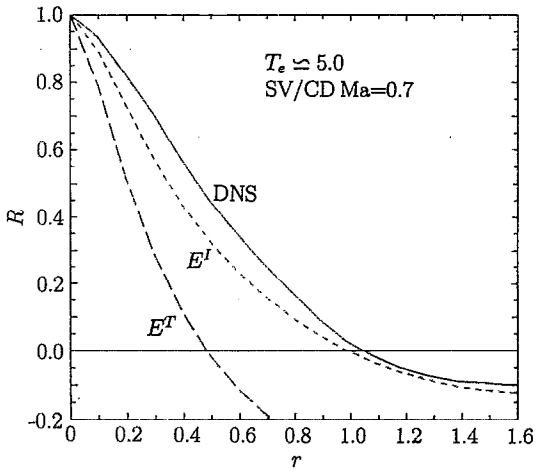

FIG. 15. Variation of scalar correlation R with separation distance r for the M_s=0.7 SV/CD simulation. DNS results are compared with results from an EDQNM model using total turbulence energy (E^T) and solenoidal part of turbulence energy (E^I). Results in this figure were obtained at $T_e \simeq 5.0$.

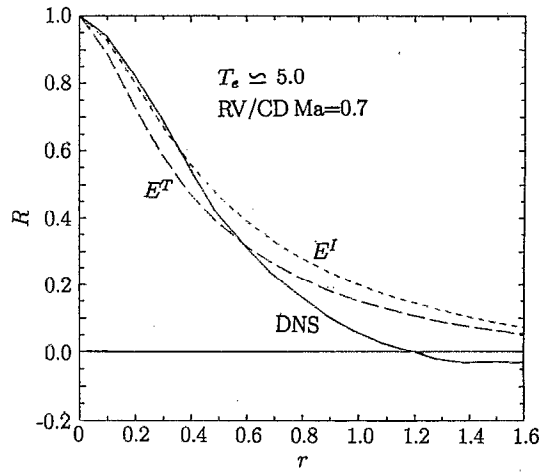

FIG. 17. Variation of scalar correlation R with separation distance r for the M_s=0.7 RV/CD simulation. DNS results are compared with results from an EDQNM model using total turbulence energy (E^T) and solenoidal part of turbulence energy (E^I). Results in this figure were obtained at $T_e \simeq 5.0$.

quence of the oscillatory behavior discussed earlier in this section. Finally, because these computations are two dimensional and compressible, a situation in which this EDQNM model is untested, one must be cautious about drawing definite conclusions from them.

ACKNOWLEDGMENTS

This work was supported by the National Science Foundation under Grant No. CTS 9221630, which we gratefully acknowledge. We will also like to express our appreciation to Professor C.-W. Shu of Brown University, Rhodes Island, for giving us the computer program on which ours is based.

[1]G. Erlebacher, M. Y. Hussaini, H. O. Kreiss, and S. Sarkar, "The analysis and simulation of compressible turbulence," Theor. Comput. Fluid Dyn. **2**, 73 (1990).
[2]S. Kida and S. Orszag, "Energy and spectral dynamics in forced compressible turbulence," J. Sci. Comput. **5**, 85 (1990).
[3]S. Ghosh and W. H. Matthaeus, "Low Mach number two-dimensional hydrodynamic turbulence: Energy budget and density fluctuations in a polytropic fluid," Phys. Fluids A **4**, 148 (1991).
[4]G. P. Zank and W. H. Matthaeus, "The equations of nearly incompressible fluids. 1. Hydrodynamics, turbulence, and waves," Phys. Fluids A **3**, 69 (1991).
[5]V. Eswaran and E. E. O'Brien, "Simulations of scalar mixing in grid turbulence using an eddy-damped closure model," Phys. Fluids A **1**, 537 (1989).
[6]A. Harten, B. Enquist, S. Osher, and S. Chakravarthy, "Uniformly high order essentially non-essentially schemes, III," J. Comput. Phys. **71**, 231 (1987).
[7]C.-W. Shu and S. Osher, "Efficient implementation of essentially non-oscillatory shock-capturing schemes," J. Comput. Phys. **77**, 439 (1988).
[8]C.-W. Shu and S. Osher, "Efficient implementation of essentially non-oscillatory shock-capturing schemes, II," J. Comput. Phys. **83**, 32 (1989).
[9]C.-W. Shu, "Numerical experiments on the accuracy of ENO and modified ENO schemes," J. Sci. Comput. **5**, 127 (1990).
[10]C.-W. Shu, T. A. Zang, G. Erlebacher, D. Whitaker, and S. Osher, "High-order ENO schemes applied to two- and three-dimensional compressible flow," J. Appl. Num. Math. **9**, 45 (1992); also ICASE Report No. 91-38, 1991.
[11]H. Tennekes and J. L. Lumley, *A First Course in Turbulence* (MIT Press, Cambridge, MA, 1972).
[12]E. E. O'Brien and G. C. Francis, "A consequence of the zero fourth cumulant approximation," J. Fluid Mech. **13**, 369 (1962).
[13]R. Childs, D. Nixon, L. Keefe, and L. Rodman, "A study of compressible turbulence," 31st Aerospace Sciences Meeting, Paper No. AIAA 93-0659, 1993.
[14]G. A. Blaisdell, N. N. Mansour, and W. C. Reynolds, "Compressibility effects on the passive scalar flux within homogeneous turbulence," Phys. Fluids **6**, 3498 (1994).
[15]G. K. Batchelor, *Theory of Homogeneous Turbulence* (Cambridge University Press, Cambridge, 1953).
[16]M. Larcheveque and M. Lesieur, "The application of eddy damped Markovian closures to problems of dispersion of particle pairs," J. Méch. **20**, 113 (1981).
[17]T. L. Jiang and E. E. O'Brien, "Simulation of scalar mixing by stationary isotropic turbulence," Phys. Fluids A **3**, 1612 (1991).
[18]J. E. Moyal, "The spectra of turbulence in a compressible fluid; Eddy turbulence and random noise," Math. Proc. Cambridge Philos. Soc. **48**, 329 (1952).
[19]S. Kida and S. Orszag, "Energy and spectral dynamics in forced compressible turbulence," J. Sci. Comput. **5**, 85 (1990).
[20]J. C. Bowman, J. A. Krommes, and M. Ottaviani, "The realizable Markovian closure. 1. General theory, with application to three wave dynamics," Phys. Fluids B **5**, 3558 (1993).